Material-Point-Method Analysis of Collapsing Slopes

**

Andersen, Søren; Andersen, Lars

Published in:
Computational Geomechanics : COMGEO I

Publication date:
2009

Document Version
Publisher's PDF, also known as Version of record

MATERIAL-POINT-METHOD ANALYSIS OF COLLAPSING SLOPES

S.M. Andersen & L. Andersen
Department of Civil Engineering, Aalborg University, Aalborg, Denmark

ABSTRACT: *To understand the dynamic evolution of landslides and predict their physical extent, a computational model is required that is capable of analysing complex material behaviour as well as large strains and deformations. Here, a model is presented based on the so-called generalised-interpolation material-point method, combining a Eulerian grid for solving the governing equations of a continuum with a Lagrangian description for the material. The method is extended to analyse interaction between multiple bodies, introducing a master–slave algorithm for frictional contact along interfaces. Further, a deformed material description is introduced, based on time integration of the deformation gradient and utilising Gauss quadrature over the volume associated with each material point. The method has been implemented in a Fortran code and employed for the analysis of a landslide that took place during the night of December 1st, 2008, near Lønstrup, Denmark. Using a simple Mohr-Coulomb model for the soil, the computational model is able to reproduce the change in the slope geometry at the site.*

1 INTRODUCTION

Slope stability and the initiation of landslides can be analysed using classical geotechnical methods or, for example, finite-element analysis (FEA). However, to model the behaviour of the soil during a slide, a computational method must be able to handle dynamic problems involving large strains and displacements as well as complex material behaviour. To avoid the mesh entanglement associated with Lagrangian FEA or the mass diffusion encountered in Eulerian descriptions, a novel computational technique for modelling landslides is presented. The numerical model is an extension of the material-point method (MPM) (Sulsky, Chen, & Schreyer 1994; Sulsky, Zhou, & Schreyer 1995) and the generalised-interpolation material-point (GIMP) method (Bardenhagen & Kober 2004). In the material-point method, the physical domain is discretized into a number of points where material properties and state variables are prescribed. The interaction between the different points and the development of stresses and strains are obtained by mapping to a grid when solving the governing equations. As the material points carry all the state variables, an undeformed mesh can be employed throughout the analysis. Also, convection issues associated with a traditional Eulerian formulation are avoided.

In the original MPM formulation (Sulsky, Chen, & Schreyer 1994), mapping between the material points and the grid is performed by evaluating the nodal shape functions associated with the grid at the location of the material points. Associating a volume with each material point, and integrating over these volumes when mapping between the material points and the grid, is shown by Bardenhagen et al. (2001) to provide more accurate results. For an undeformed material-point volume, the integration can be carried out analytically. However, when the material points are

subject to significant strains and rotations, integration in the deformed state may be necessary. For this purpose a method is proposed in which a Gauss quadrature rule is employed for the numerical integration over the deformed volume defined by the deformation gradient tensor at the material point.

In order to model the interaction between different bodies, a contact algorithm is introduced. The governing equations are solved separately for each individual continuum and the interaction between different materials is governed by a frictional contact law, enforcing no interpenetration of adjacent materials and allowing materials to slide relatively to each other. The evaluation of the contact forces is performed on the computational grid. In the original work presented by York et al. (1999) and Bardenhagen et al. (2000, 2001), the normal vectors for each continuum are found independently, by employing the grid-node density field obtained for each individual continuum. Due to the spatial discretization of the material, the normal vectors of two adjacent bodies may not point exactly in opposite directions and therefore this approach may fail. In particular, sliding at an interface can be hindered by an erroneous prediction of the outward normal on parts of the surface of a small body interacting with a body with a much greater extent. In order to avoid this, a change of the original algorithm is presented that allows the interaction between bodies with an arbitrary interface. This is done by defining a hierarchy of bodies, and letting the normal vector for the master surface define the direction of the common interface.

The theory behind the numerical model is presented in Section 2. Section 3 presents a numerical study of a specific land slide taking place on the coastline at Lønstrup in northern Denmark December 1st, 2008. Finally, the conclusions are presented in Section 4.

2 THEORY AND IMPLEMENTATION

Consider a continuum subject to initial and boundary conditions. The governing equation for the momentum is given by

$$\rho \frac{dv_\alpha}{dt} = \frac{\partial \sigma_{\alpha\beta}}{\partial x_\beta} + \rho b_\alpha, \tag{1}$$

where $\sigma_{\alpha\beta}$ is the Cauchy stress tensor and b_α is the specific body force. The index α ranges over 1 and 2 in the case of plane strain considered in the present analysis.

A weak form of Eq. (1) is obtained by multiplying the balance of momentum by an arbitrary test function w_α and integrating over the initial volume. Applying integration by parts and employing the Green theorem, the weak form is given by

$$\int_\Omega \rho w_\alpha \frac{dv_\alpha}{dt} dV = \int_{\Gamma_\tau} w_\alpha \tau_\alpha d\Gamma - \int_\Omega \frac{\partial w_\alpha}{\partial x_\beta} \sigma_{\alpha\beta} dV + \int_\Omega \rho w_\alpha b_\alpha dV, \tag{2}$$

where τ_α is the surface traction on part of the boundary, Γ_τ, where the surface tractions are prescribed, and Ω the physical domain.

2.1 Generalized interpolation material-point discretization

In order to discretize Eq. (2), the domain is divided into n_p subdomains Ω_p, $p = 1, 2, \ldots, n_p$. A material point is placed at the centre of each subdomain, defined by the coordinates x_α^p, $p = 1, 2, \ldots, n_p$. The velocities v_α^p and the stresses $\sigma_{\alpha\beta}^p$ as well as the external body forces b_α^p at the n_p material points are defined as volume-weighted quantities, i.e.

$$v_\alpha^p = \frac{1}{V_p} \int_{\Omega_p} v_\alpha(x_\beta) dV, \quad \sigma_{\alpha\beta}^p = \frac{1}{V_p} \int_{\Omega_p} \sigma_{\alpha\beta}(x_\gamma) dV, \quad b_\alpha^p = \frac{1}{V_p} \int_{\Omega_p} b_\alpha(x_\beta) dV. \tag{3}$$

Similarly, a deformation gradient is associated with each material point in the current state as

$$F^p_{\alpha\beta} = \left.\frac{\partial x_\alpha}{\partial x^0_\beta}\right|_{x=x_p} = \frac{1}{V_p}\int_{\Omega^p} F_{\alpha\beta}(x_\gamma)dV, \tag{4}$$

where x_0 are the initial coordinates.

In order to obtain a discrete spatial representation, particle characteristic functions, χ_p, associated with the material points are defined (Bardenhagen & Kober 2004). The particle characteristic functions are normalized with respect to the initial volume, i.e.

$$\int_{\Omega^p_0} \chi_p(x_\alpha, t)d\Omega = V^0_p, \tag{5}$$

where V^0_p is the volume associated with the material point in the initial state. Field quantities are represented as sums over the material points, i.e.

$$f(x_\alpha) \simeq \sum_p f_p \chi_p(x_\alpha). \tag{6}$$

For example, the first term in the balance of momentum is represented by

$$\rho\frac{dv_\alpha}{dt} \simeq \sum_p \rho^p \frac{dv^p_\alpha}{dt}\chi_p = \sum_p \frac{m_p}{V_p}\frac{dv^p_\alpha}{dt}\chi_p = \sum_p \frac{\dot\pi^p}{V_p}\chi_p, \tag{7}$$

where the momentum rate of change has been introduced as $\dot\pi^p = m_p dv^p_\alpha/dt$. In our implementation we use a constant particle characteristic function. Hence, stresses, densities etc. are considered constants within the volume associated with each material point.

Using the material-point representation in the balance of momentum yields

$$\begin{aligned}\sum_p \frac{\dot\pi^p_\alpha}{V_p}\int_{\Omega_p \bigcup \Omega} w_\alpha \chi_p dV = &\int_{\Gamma_\tau} w_\alpha \tau_\alpha dS \\ &- \sum_p \sigma^p_{\alpha\beta}\int_{\Omega_p \bigcup \Omega}\frac{\partial w_\alpha}{\partial x_\beta}\chi_p dV + \sum_p \frac{m^p b^p_\alpha}{V_p}\int_{\Omega_p \bigcup \Omega} w_\alpha \chi_p dV.\end{aligned} \tag{8}$$

The left-hand side represents the rate of change of momentum. On the right-hand side, the first term represents the surface tractions, the second term represents internal forces due to stress gradients, while the last term represents external body forces. Further it is noted that the physical quantities are evaluated at each material point.

A background grid is introduced and the test function $w_\alpha(x_\beta, t)$ is discretized into its values w^i_α, $i = 1, 2..n_n$ at n_n nodes. Within each cell of the grid, interpolation of the test function and its gradient is carried out by means of shape functions $N_i(x_\beta)$ associated with the nodes, i.e

$$w_\alpha(x_\beta) \simeq \sum_i w^i_\alpha N_i(x_\beta), \quad \frac{\partial w_\alpha(x_\gamma)}{\partial x_\beta} \simeq \sum_i w^i_\alpha \frac{\partial N_i(x_\gamma)}{\partial x_\beta}, \tag{9}$$

where $\sum_i$ denotes the sum over the grid nodes and N_i is the nodal shape function associated with node i. Employing Eq. (9), the balance of momentum can be written as

$$\begin{aligned}\sum_i\sum_p w^i_\alpha \dot\pi^p_\alpha \frac{1}{V_p}\int_{\Omega_p \bigcup \Omega} N_i \chi_p dV = &\sum_i w^i_\alpha \int_{\Gamma_\tau} N_i \tau_\alpha dS \\ - \sum_i\sum_p w^i_\alpha \sigma^p_{\alpha\beta}\int_{\Omega_p \bigcup \Omega}\frac{\partial N_i}{\partial x_\beta}\chi_p dV &+ \sum_i\sum_p w^i_\alpha m^p b^p_\alpha \frac{1}{V_p}\int_{\Omega_p \bigcup \Omega} N_i \chi_p dV.\end{aligned} \tag{10}$$

Now the weighting and the gradient-weighting functions are introduced as

$$\bar{N}_{ip} = \frac{1}{V_p}\int_{\Omega_p \bigcup \Omega} N_i \chi_p dV, \quad \frac{\partial \bar{N}_{ip}}{\partial x_\beta} = \frac{1}{V_p}\int_{\Omega_p \bigcup \Omega} \frac{\partial N_i}{\partial x_\beta}\chi_p dV. \tag{11}$$

Utilising that the test functions w_α^i are arbitrary, the system of equations need to be satisfied at all grid nodes. Employing Eq. (11) in Eq. (10) yields

$$\sum_p \dot{\pi}_\alpha^p \bar{N}_{ip} = \int_{\partial\Omega_\tau^0} N_i \tau_\alpha dS - \sum_p \sigma_{\alpha\beta}^p V_p \frac{\partial \bar{N}_{ip}}{\partial x_\beta} + \sum_p m^p b_\alpha^p \bar{N}_{ip}. \tag{12}$$

Rewriting the balance of momentum yields

$$\dot{\pi}_\alpha^i = f_\alpha^{i,int} + f_\alpha^{i,ext}, \tag{13}$$

where

$$\dot{\pi}_\alpha^i = \sum_p \dot{\pi}_\alpha^p \bar{N}_{ip}, \quad f_\alpha^{i,int} = -\sum_p \sigma_{\alpha\beta}^p V_p \frac{\partial \bar{N}_{ip}}{\partial x_\beta}, \quad f_\alpha^{i,ext} = \int_{\Gamma_\tau} N_i \tau_\alpha dS + \sum_p m^p b_\alpha^p \bar{N}_{ip} \tag{14}$$

are the rate of change of the nodal momentum, the internal force and the external force, respectively. As the mass is tracked through the material points, the conservation of mass is automatically satisfied.

2.2 Numerical integration in the deformed state

The above derivation yields final equations identical to the GIMP formulation presented by Bardenhagen & Kober (2004). For landslides involving rotations and deformations the analytically evaluated GIMP weighting functions in (Bardenhagen & Kober 2004) can no longer be applied to represent the physical domain of the material points. Hence, a scheme for numerically evaluating the GIMP functions is presented. The subdomain associated with each material point is assigned a number of Gauss points. Rewriting the integral part of the weighting functions and the gradient weighting functions as sums over the Gauss points yields

$$\bar{N}_{ip} = \frac{1}{V_p}\sum_{GP} \chi_p(x_\alpha^{GP}) N_i(x_\alpha^{GP}) \phi_{GP}, \quad \frac{\partial \bar{N}_{ip}}{\partial x_\beta} = \frac{1}{V_p}\sum_{GP} \chi_p(x_\alpha^{GP}) \left.\frac{\partial \bar{N}_{ip}(x_\alpha)}{\partial x_\beta}\right|_{x_\alpha = x_\alpha^{GP}} \phi_{GP}, \tag{15}$$

where ϕ_{GP} is the weight for the Gauss point, normalised to provide $\sum_{GP} \phi_{GP} = V_p$. Integrating numerically over the shared domain is consistent as either $N_i(x_\alpha^{GP}) = 0$ or $\chi_p(x_\alpha^{GP}) = 0$ outside the shared domain. The equations can be further simplified as

$$\bar{N}_{ip} = \sum_{GP} \chi_p(x_\alpha^{GP}) N_i(x_\alpha^{GP}) \bar{\phi}_{GP}, \quad \frac{\partial \bar{N}_{ip}}{\partial x_\beta} = \sum_{GP} \chi_p(x_\alpha^{GP}) \left.\frac{\partial \bar{N}_{ip}(x_\alpha)}{\partial x_\beta}\right|_{x_\alpha = x_\alpha^{GP}} \bar{\phi}_{GP}, \tag{16}$$

where $\sum_{GP} \bar{\phi}_{GP} = 1$. If a single Gauss point, located at the material point, is employed, the weighting function becomes simply the nodal shape function and the original MPM formulation given by Sulsky et al. (1995) is retrieved.

Considering a material point initially located at $x_\alpha^{p,0}$, the coordinate for a Gauss point can be written as

$$x_\alpha^{GP,0} = x_\alpha^{p,0} + dx_\alpha^0, \tag{17}$$

where $x_\alpha^{GP,0}$ is the location of the Gauss point in the initial configuration and dx_α^0 is the line segment between the material point and the Gauss point in the initial configuration. At an arbitrary time the location of the Gauss point is given as

$$x_\alpha^{GP} = x_\alpha^p + dx_\alpha. \tag{18}$$

Using the deformation gradient $F_{\alpha\beta}$, the deformed line segment dx_α can be calculated by

$$dx_\alpha = F_{\alpha\beta} dx_\beta^0, \qquad F_{\alpha\beta} = \frac{\partial x_\alpha}{\partial \xi_\gamma} \frac{\partial \xi_\gamma}{\partial \xi_\delta^0} \frac{\partial \xi_\delta^0}{\partial x_\beta^0}. \tag{19}$$

In the presented examples, the initial local axes are chosen along the global coordinate system. Hence, in this case $F_{\alpha\beta} = \partial \xi_\alpha / \partial \xi_\beta^0$. The idea of utilising a non-linear strain measure within the MPM is introduced by Guilkey & Weiss (2003) who introduce a weak form of the balance of momentum based on the deformation gradient and the second Piola-Kirchhoff stress tensor.

The location of the Gauss points is specified through the deformation-gradient tensor which needs to be tracked for each material point through the simulation. In the initial configuration, the deformation-gradient tensor is presumed known. Typically, an undeformed material state will be prescribed, i.e. $F_{\alpha\beta}^0 = \delta_{\alpha\beta}$, where $\delta_{\alpha\beta}$ is the Kronecker delta. An explicit forward difference scheme for updating the deformation gradient is employed,

$$F_{\alpha\beta}^{k+1} = \Delta F_{\alpha\beta}^{k+1} F_{\alpha\beta}^k. \tag{20}$$

Expressing the time derivative of the deformation gradient as $\partial F_{\alpha\beta}/\partial t = \partial v_\alpha^k / \partial x_\beta^0$, $\Delta F_{\alpha\beta}^k$ can be expressed as

$$\Delta F_{\alpha\beta}^{k+1} = \delta_{\alpha\beta} + \Delta t \frac{\partial v_\alpha^k}{\partial x_\beta}. \tag{21}$$

Using the nodal shape functions, the change in deformation gradient at an arbitrary point x_γ can be evaluated as

$$\Delta F_{\alpha\beta}^{k+1}(x_\gamma) = \delta_{\alpha\beta} + \Delta t \sum_i v_\alpha^{i,k} \frac{\partial N_i(x_\gamma)}{\partial x_\beta}. \tag{22}$$

By use of the particle characteristic function the increment of deformation gradient can be formulated as

$$\Delta F_{\alpha\beta}^{p,k+1} = \delta_{\alpha\beta} + \Delta t \sum_i v_\alpha^{i,k} \frac{\partial \bar{N}_{ip}}{\partial x_\beta}. \tag{23}$$

This way of integrating the deformation gradient, using the grid velocities, is also employed by Love & Sulsky (2006).

The stress is integrated using an updated Lagrangian scheme. At the beginning of the time step, a reference state is defined by $S_{\alpha\beta}^k := \sigma_{\alpha\beta}^k$. For small strain increments, the approximation $\dot{\varepsilon}_{\alpha\beta} = \dot{E}_{\alpha\beta}$ is valid, where $\dot{E}_{\alpha\beta}$ is the Green strain rate and $\dot{\varepsilon}_{\alpha\beta}$ is the linear strain rate,

$$\dot{\varepsilon}_{\alpha\beta} = \frac{1}{2} \left(\frac{\partial v_\alpha}{\partial x_\beta} + \frac{\partial v_\beta}{\partial x_\alpha} \right). \tag{24}$$

Thus the rate of change of the second Piola-Kirchhoff stress tensor is given by

$$\dot{S}_{\alpha\beta} = C_{\alpha\beta\gamma\delta} \dot{\varepsilon}_{\gamma\delta}, \tag{25}$$

where $C_{\alpha\beta\gamma\delta}$ yields the constitutive behaviour of an observed material point at the current material state. Using a forward difference scheme the Piola-Kirchhoff stress at the end of the time step is approximated by

$$S_{\alpha\beta}^{k+1} = \sigma_{\alpha\beta}^{k} + \Delta t \dot{S}_{\alpha\beta} \tag{26}$$

The local deformation occurring during the time step is given by $\Delta F_{\alpha\beta}^{k}$. Hence, with $\Delta J = \det(\Delta F_{\alpha\beta}^{k+1})$, the rate objective Cauchy stress at end of the time step is given by

$$\sigma_{\alpha\beta}^{k+1} = \frac{1}{\Delta J} \Delta F_{\alpha\gamma}^{k+1} S_{\gamma\delta}^{k+1} \Delta F_{\delta\beta}^{k+1}. \tag{27}$$

2.3 Implementation of the improved GIMP algorithm

In the subsections above, the governing equations for a large-strain GIMP method using numerical integration are given. The basic idea is to solve the balance of momentum on the grid and then use the information to update the state variables at the material points. The mass and momentum at a grid node i are found by

$$m_i^k = \sum_p m_p^k \bar{N}_{ip}, \quad \pi_\alpha^{i,k} = \sum_p \pi_\alpha^{p,k} \bar{N}_{ip}, \tag{28}$$

respectively. Using a linear extrapolation of Eq. (13), the nodal momentum at the end of the time step becomes

$$\pi_\alpha^{i,k+1} = \pi_\alpha^{i,k} + \Delta t (f_\alpha^{i,int,k} + f_\alpha^{i,ext,k}). \tag{29}$$

The position and velocity updates for the material points are then given by

$$x_\alpha^{p,k+1} = x_\alpha^{p,k} + \frac{\Delta t}{m_p} \sum_i \pi_\alpha^{i,k+1} \bar{N}_{ip}, \quad v_\alpha^{p,k+1} = v_\alpha^{p,k} + \frac{\Delta t}{m_p} \sum_i (f_\alpha^{i,int,k} + f_\alpha^{i,ext,k}) \bar{N}_{ip}. \tag{30}$$

The algorithm can be summarised as:

1. Initialisation of material properties, including the deformation gradient at the material points at time $t^k = 0$
2. At each time step:
   - A background computational grid is generated
   - The coordinates for the Gauss points are found by Eq. (18)
   - The weighting and gradient-weighting functions are determined by Eq. (16)
   - Stress and strain increments are found and the stresses and strains are updated
   - The objective Cauchy stresses at the end of the time step are found by Eq. (27)
   - Internal and external forces are found by Eq. (14)
   - The updated nodal momentum is determined using Eqs. (14) and (29)
   - The position and the velocity of the material points are found by Eq. (30)
   - The deformation gradient increment for the material points are updated using Eq. (20), and the total deformation gradient is calculated.

Here, an algorithm as simple as possible has been presented. Hence, explicit forward difference schemes are employed for updating the deformation gradient, Eq. (23), as well as the stress, Eq. (26), and to update the velocity and the position of the material points, Eq. (30). As the resulting equations are similar to the original MPM formulation, the difference relates to the construction of the weighting functions and how to integrate the constitutive behaviour. Alternatively, implicit MPM schemes presented by, for example, Cummins & Brackbill (2002), Guilkey & Weiss (2003), or Sulsky & Kaul (2004) can be implemented.

2.4 Frictional contact algorithm for multiple interfaces

The algorithm described above is employed when the modelled material can be considered one single continuum. According to Sulsky et al. (1995), the algorithm can also model collision between colliding bodies, illustrated by the simple problem of collision of two elastic discs. This is due to the interaction between the two bodies when internal forces are calculated on the grid. However, York et al. (1999) showed that modelling interaction between different bodies has shortcomings when using a shared nodal field for the whole domain. If two particles are in contact over a large area compared to the volume, or if the materials are soft, the two interacting materials tend to stick together instead of separating after contact. York et al. (1999) provide an algorithm that only allows bodies to share grid nodes when they are moving towards each other.

In the present study of landslides it is essential to model friction at interfaces. Further, the large deformations necessitate the ability to model material separation, when parts of the soil stop belonging to the continuum, and is able to move relatively to the remaining soil. Hence, a frictional contact algorithm is introduced, based on the work by Bardenhagen et al. (2000, 2001). Thus, the domain of material points is subdivided into a number of subdomains (so-called 'grains') in the initial reference. Within each subdomain, the equations for a continuum are valid. The interpolations defined by Eqs. (28) and (14) are performed for each continuum. Between adjacent continua, a frictional contact model is introduced. Using $v_\alpha^i = \pi_\alpha^i / m_i$, a centre-of-mass velocity, $v_\alpha^{i,CM}$, at a grid node can be found by integrating over all material points. Similarly, the velocity of one continuum, $v_\alpha^{i,c}$, can be found, where index c corresponds to the continuum material. Nodes representing interfaces are identified by

$$v_\alpha^{i,CM} - v_\alpha^{i,c} \neq 0. \tag{31}$$

For a node at an interface, a normal surface traction, $\tau_n^{i,c}$, is introduced by $\tau_n^{i,c} = n_\alpha^{i,c} \sigma_{\alpha\beta}^{i,c} n_\beta^{i,c}$, where $n_\alpha^{i,c}$ is the outward unit normal of continuum c evaluated at node i, and $\sigma_{\alpha\beta}^{i,c}$ is the Cauchy stress at the node found by mapping from the material points.

The contact forces are determined at the grid nodes. Direction-of-sliding forces and normal forces applied to the continuum at a grid node are determined based on unit outward normal vectors. An algorithm for determining these normal vectors based on the density fields is presented in (York, Sulsky, & Schreyer 1999). In order to model problems, in which three or more continua interact, a master–slave relationship is employed. The continua at a grid node are assigned numbers, where $c = 1$ corresponds to the master material. For material 1, the normal vector $n_\alpha^{i,1}$ is determined according to the original scheme proposed by York et al. (1999). The normal vector for material 2 is prescribed as $n_\alpha^{i,2} = -n_\alpha^{i,1}$, i.e. orthogonal to the density field of material 1 along the common interface. The normal vector for material 3 is prescribed orthogonal to the combined density fields of materials 1 and 2. This can be generalised to handle any number of continua.

The normal surface traction is found as described in (Bardenhagen, Guilkey, Roessig, Brackbill, Witzel, & Foster 2001). Using the sign convention where compressive stresses are negative, the frictional-contact algorithm is enforced at an interface node when $t_n^{i,c} < 0$.

When continua are not in contact, the governing equation (13) is solved for each body on its own. When the bodies are moving towards each other, frictional contact is enforced by changing the velocity fields of each continuum in order to prevent interpenetration and allow for incorporation of frictional forces. The details in the numerical implementation are found in the work by Bardenhagen et al. (2001). Basically, the algorithm prevents sliding when $t_t^{i,c} < \mu t_n^{i,c}$, where $t_t^{i,c}$ is the unit traction vector resolved in the tangential direction of sliding and μ is the coefficient of friction between the continuum and the other materials it is interacting with. When $t_t^{i,c} = \mu t_n^{i,c}$, sliding is allowed and the frictional force is determined by the coefficient of friction.

3 CASE STUDY: COLLAPSING SLOPE ON THE COAST NEAR LØNSTUP

3.1 Presentation of the physical problem

The presented method is employed to analyse a recent event of a major landslide on the coastline between Lønstrup and Rubjerg Knude in northern Denmark. The local soil consist of interchanging layers of clay and sand, originally deposited almost horizontally. However, due to tectonic dislocations during the Weichsel glaciation, the layers are now inclined at angles as high as 60 degrees (Pedersen 2006). This has a significant impact on the slope stability, and smaller but similar landslides are often reported in the area (Skov og Naturstyrelsen 2008), typically observed at the interfaces between different layers.

The slide near Rubjerg Knude occurred in the night between November 30th and December 1st, 2008, and was most likely triggered by a heavy rainfall. According to Bent Lykkegaard, responsible for the maintenance of the coastline area, the clay became heavier, eventually causing it to slide along the interface with sand (Tv2|Nord 2008). On December 3rd, 2008, a survey was carried out in order to determine the geometry of the collapsed slope. Figure 1 (left) shows a photograph taken from the top of the collapsed slope. Already on November 27th, 2008, deep cracks were observed, but it was expected that it would take several years for the cracks to develop into a slide. A photograph of typical cracks, probably due to initial sliding in an interface between clay and sand, about 300 metres to the south of the slide, is shown in Fig. 1 (right).

Fig. 1. Left: The slope near Lønstrup after the landslide (December 3rd, 2008). The poles in the photograph are used as points in the land surveying performed. Right: Development of cracks in the sand material (December 3rd, 2008). The photograph is taken approximately 300 metres to the south of the slide.

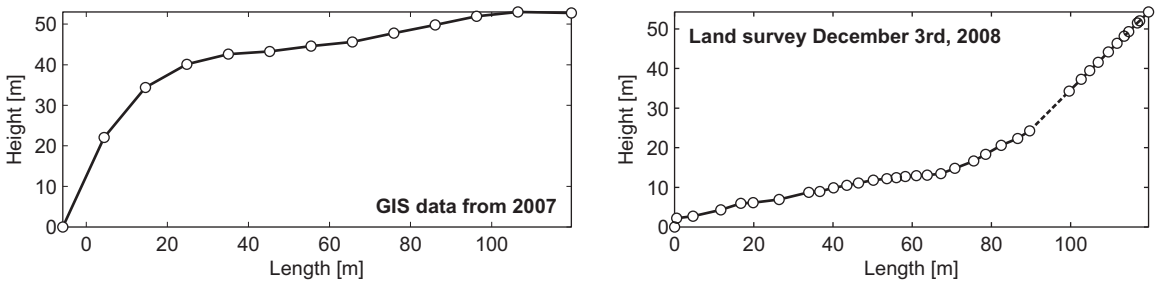

Fig. 2. Comparison of the slope geometry at the site near Lønstrup before and after the slide based on GIS data from 2007 (left) and land surveying performed December 3rd, 2008 (right).

After the field trip, the data obtained from the survey was compared to GIS data from 2007. Figure 2 shows the cross sections before and after the slide. Some of the survey poles, utilised for obtaining the slope geometry after the slide, are visible in Fig. 1 (left). The relative position of the two cross sections, shown in Fig. 2, are subject to uncertainty. The location of a reference point on the slope after the slide was obtained using a simple GPS transmitter is with an uncertainty ± 12m at the point of measuring, while the resolution of the GIS data is 10 metres. Nonetheless, the figure clearly shows the extent of the slide and a significant change in the slope geometry.

3.2 Material model for the soil

A major difficulty in obtaining a reliable numerical analysis of the particular slide is the complex material properties and the identification of layer boundaries present in the slope. In the considered problem, the soil consists of a complex pattern of clay and different sand materials. Further, the material properties, at the initiation of the slide, are uncertain. Another limitation is the lack of constitutive models involving very large deformations for soil materials. In order to test the frictional contact model and to study the suggested failure mechanism reported in (Tv2|Nord 2008), a numerical model with simplified material assumptions is employed. By introducing simplified material and geometrical models, the soil is represented as two isotropic, homogenous materials, clay and sand. The clay and sand are modelled as different continuum materials. The interaction between the materials is described using the frictional-contact algorithm.

Both the sand and the clay are modelled as elasto-plastic materials, based on the Mohr-Coulomb yield criterion. Thus, a yield function f is introduced such that $f < 0$ corresponds to elastic material behaviour, whereas elasto-plastic behaviour is observed when $f = 0$. In terms of principal stresses by, the yield criterion reads:

$$f = \frac{1}{2}(\sigma_3 - \sigma_1) + \frac{1}{2}(\sigma_1 + \sigma_3)\sin\phi - c\cos\phi \leq 0, \tag{32}$$

where ϕ is the angle of friction and c is the cohesion. In Equation (32), tension is considered positive and the principal stresses are ordered as $\sigma_1 \leq \sigma_2 \leq \sigma_3$. The stress rate is given in terms of the elastic strain rate, i.e.

$$\dot{\sigma}_{\alpha\beta} = E_{\alpha\beta\gamma\delta} : (\dot{\varepsilon}_{\gamma\delta} - \dot{\varepsilon}^p_{\gamma\delta}), \tag{33}$$

where $\dot{\varepsilon}_{\gamma\delta}$ is the total strain rate, $\dot{\varepsilon}^p_{\gamma\delta}$ is the plastic rate and $E_{\alpha\beta\gamma\delta}$ is the elastic constitutive tensor. In the case of linear isotropic elasticity, $E_{\alpha\beta\gamma\delta}$ depends on Young's modulus, E, and Poisson's ratio, ν. Assuming non-associated plasticity, the plastic strain increment is found as

$$\dot{\varepsilon}^p_{\alpha\beta} = \dot{\lambda}\frac{\partial g}{\partial \sigma_{\alpha\beta}}, \quad g = \frac{1}{2}(\sigma_3 - \sigma_1) + \frac{1}{2}(\sigma_1 + \sigma_3)\sin\psi. \tag{34}$$

where $\dot{\lambda}$ is a positive scaling factor, and g is the plastic potential with ψ denoting the angle of dilatation of the soil. In the numerical solution, finite increments in the strain are considered. Hence, the state of stress may initially be taken outside the yield surface. In order to return the stresses to a physically valid state, the efficient return algorithm proposed by Clausen et al. (2006) is applied for the Mohr-Coulomb criterion.

The clay is assumed to be undrained, represented by the material properties: $E = 20$ MPa, $\nu = 0.40$, $\rho_0 = 1900$ kg/m^3, $c = 100kPa$, $\phi = 1^\circ$, and $\psi = 0^\circ$. The sand is assumed drained with the initial properties: $E = 20$ MPa, $\nu = 0.40$, $\rho_0 = 1900$ kg/m^3, $c = 0$, $\phi = 35^\circ$, and $\psi = 5^\circ$. Further, the interface between sand and clay is modelled with an coefficient of friction $\mu = 0.6$.

This corresponds to requiring a smaller force in order to enforce sliding at the interface than to trigger plastic response in the sand next to the interface, as $\tan 35^\circ \approx 0.7$.

During the landslide, significant plastic shear strains are accumulated in the sand. This leads to over-excessive dilatation if the material model is used uncritically. To avoid this, dilation cut-off is implemented when the maximum void ratio for the sand has been reached. The cut-off condition is implemented numerically by representing all material points that have obtained the maximum void ratio as a new continuum. This allows the loose sand to slide relatively to the underlying sand. In the present case, an initial void ratio of 0.5 is assumed and the maximum void ratio is estimated to 0.8. A more realistic model would consider the effects of capillary tension in the sand as well as the curvature of the yield function at low confining pressures, i.e. near the ground surface. The use of more accurate material models is the focus of future research.

3.3 Simulation of the landslide—results and discussion

A two-dimensional cross section is divided into a number of rectangular domains each represented by a material point (either clay or sand). The model has 80 computational cells in the horizontal direction and 32 cells in the vertical direction, see Figure 3. The geometry for the part of the numerical model representing the slope is obtained from the GIS data. The part of the model to the left of the slope, that represents the beach and the seabed, is modelled with an inclination of 6%. Three by three material points are defined for each cell in the computational grid, leading to a total of 10977 material points in the model in the initial configuration.

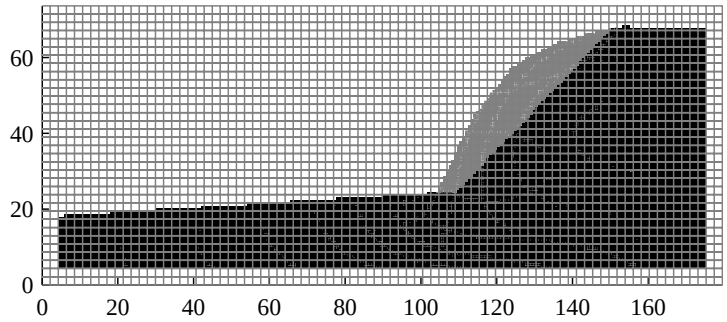

Fig. 3. The configuration of material points before the slide. The mesh visible is the computational grid and lengths are in metres. A total number of 10977 material point is employed in the shown model. Dark shades indicate sand and light shades indicate clay. Information from GIS data has been utilised for defining the geometry.

The initial stresses in the slope are determined using the algorithm presented by Andersen & Andersen (2008), where the gravity is gradually applied to the material points. Based on the geometry and the initial stresses, the deformed slope geometry is found by explicitly integrating in time. A time increment of $\Delta t = 0.002$ s is employed, and the simulation has been carried out until the sliding motion has ceased. In the current model, the slide takes approximately 9.0 s.

Figure 4 shows the configuration over time. The slide starts as a slip at the interface between the clay and the sand. At $t = 2.9$ s the sliding is mostly due to the clay sliding down the sand with some plastic deformations taking place in the clay. Plastic deformations in the sand is of little importance. At $t = 2.9$ s the physically dominant interface is the interface between the clay and the sand. At $t = 5.8$ s the interaction between the sand and the clay at the interface on the beach has lead to plastic deformations in the sand closest to the clay. Normal forces enforced onto the clay by the frictional contact law is now yielding a large contribution to stopping the slide.

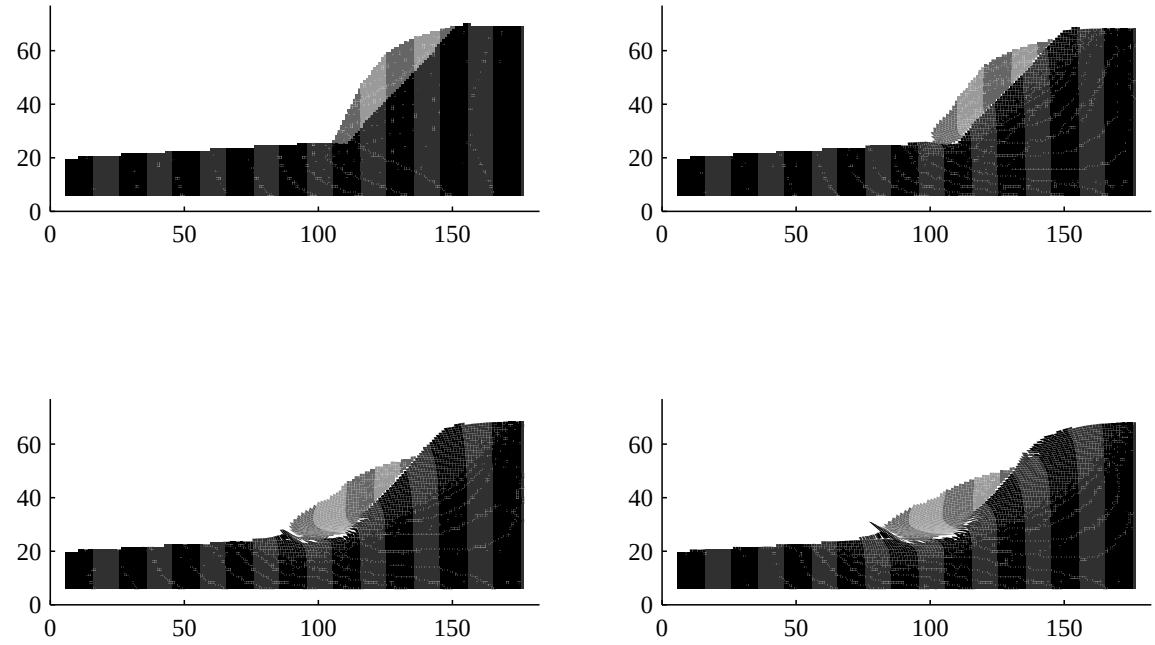

Fig. 4. The geometry of the slope at different instants of time: $t = 0$ s (upper right); $t = 2.9$ s (upper left); $t = 5.8$ s (lower right); $t = 9.0$ s (lower left). Dimensions are in metres and the (initially vertical) stripes are solely inserted to provide a better visualisation of the deformation mechanism. Dark shades indicate sand and light shades indicate clay.

Another observation to be made from that figure is the significant change in the shape of the clay. At $t = 9.0$ s, after which no further sliding is taking place, the clay has stopped at a newly formed interface between the two materials (between $x = 70$ m and $x = 90$ m). The interface has an inclination opposite to the inclination of the original slope. Hence, with the provided layer boundaries and material properties, the plastic deformations in the sand along the beach contributes in stopping the slide. Finally, comparing the solutions at $t = 5.8$ s and $t = 9.0$ s, plastic deformations are observed in the sand at the upper part of the slope, i.e. between $x = 130$ m and $x = 150$ m.

4 CONCLUSION

A new numerical technique for modelling problems involving large strains and deformations is presented. The model is an extension of the generalised-interpolation material-point method, employing numerical integration in the deformed state. Interaction between several bodies is modelled using a frictional contact algorithm based on a master–slave interface definition.

The numerical method is tested by analysing a recent landslide at the coastline near Lønstrup in northern Denmark. A two-dimensional model of the slope before the landslide is obtained using GIS data. A Mohr-Coulomb model is employed to model the elasto-plastic behaviour of the soil, using material properties representative for drained sand and undrained clay, respectively. In the simulation, the slide is initiated by increasing the density of the clay, corresponding to the behaviour during heavy rainfall. A frictional contact algorithm is employed at the interface between the clay and the sand. With the utilised material and interface properties, the landslide is triggered at the interface between the sand and the clay, whereas the elasto-plastic properties of the two materials are of a little importance regarding the initiation of the slide. However, they have a significant influence on the material deformations during the slide.

The numerical test case shows that it is possible to model elasto-plastic deformation, slide between the different materials, and the change of the sand properties due to dilatation using a fairly simple model. A model able to handle all these physical phenomena simultaneously would be extremely difficult to construct using a conventional method such as the finite element method. Despite the many simplifications in the numerical representation of the physical problem, the model provides results that are qualitatively and quantitatively similar to the slide observed on location.

REFERENCES

Andersen, S. & Andersen, L. (2008). Modelling of landslides with the material-point method. In *The Sixth International Conference on Engineering Computational Technology*, Athens, Greece. Civil-Comp Press.

Bardenhagen, S., Brackbill, J., & Sulsky, D. (2000). The material-point method for granular materials. *Computer Methods in Applied Mechanics and Engineering 187*, 529–541.

Bardenhagen, S., Guilkey, J., Roessig, K., Brackbill, J., Witzel, W., & Foster, J. (2001). An improved contact algorithm for the material point method and application to stress propagation in granular material. *CMES 2*(4), 509–522.

Bardenhagen, S. & Kober, E. (2004). The generalized interpolation material point method. *CMES 5*(6), 477–495.

Clausen, J., Damkilde, L., & Andersen, L. (2006). Efficient return algorithms for associated plasticity with multiple yield planes. *International Journal for Numerical Methods in Engineering 66*, 1036–1059.

Cummins, S. & Brackbill, J. (2002). An implicit particle-in-cell method for granular materials. *Journal of Computiatonal Physics 180*(2), 506–548.

Guilkey, J. & Weiss, J. (2003). Implicit time integration for the material point method: Quantitative and algoritmic comparisons with the finite element method. *International Journal for Numerical Methods in Engineering 57*(9), 1323–1338.

Love, E. & Sulsky, D. (2006). An unconditionally stable, energy-momemtum consistent implementation of the material point method. *Computer Methods in Applied Mechanics and Engineering 195*(33-36), 3903–3925.

Pedersen, S. (2006). Strukturer og dynamisk udvikling af Rubjerg Knude glacialtektoniske kompleks, Vendsyssel, Danmark. Technical report, Danmarks og Grønlands Geologiske Undersøgelse. In Danish.

Skov og Naturstyrelsen (2008). Jordskred ved Maarup Kirke. Webpage, www.skovognatur.dk. Information retrieved January 3rd, 2009. In Danish.

Sulsky, D., Chen, Z., & Schreyer, H. (1994). A particle method for history-dependent materials. *Computer Methods in Applied Mechanics and Engineering 118*, 179–196.

Sulsky, D. & Kaul, A. (2004). Implicit dynamics in the material-point method. *Computer Methods in Mechanics and Engineering 193*(12–14), 1137–1170.

Sulsky, D., Zhou, S., & Schreyer, H. (1995). Application of a particle-in-cell method to solid mechanics. *Computer Physics Communications 87*, 236–252.

Tv2|Nord (2008). Kæmpeskred på Rubjerg Knude. Webpage, www.tv2nord.dk. Information retrieved Dececember 29th, 2008. Interview with Bent Lykkegaard. In Danish.

York, A., Sulsky, D., & Schreyer, H. (1999). The material point method for simulation of thin membranes. *International Journal for Numerical Methods in Engineering 44*(10), 1429–1456.